# **Analysis of Convective Temperature Overturns near the East Rincon Hills Fault Zone using Semi-Analytical Models**

<sup>1</sup>Mark Person, <sup>2</sup>William D. Stone, <sup>1</sup>Melinda Horne, <sup>3</sup>James Witcher, <sup>4</sup>Shari Kelley, <sup>1</sup>Dolan Lucero, <sup>5</sup>Jesus Gomez-Velez, and <sup>6</sup>Daniel Gonzalez-Duque

<sup>1</sup>Hydrology Program, New Mexico Tech, Socorro NM, 87801

<sup>2</sup>Department of Mathematics, New Mexico Tech, Socorro NM, 87801

<sup>3</sup>Witcher and Associates, Las Cruces, NM 88003

<sup>4</sup>New Mexico Bureau of Geology and Mineral Resources, Socorro NM, 87801

<sup>5</sup>Oak Ridge National Laboratory, Oak Ridge, TN 37830

<sup>6</sup>Vanderbuilt University, Nashville, TN 37

# **Keywords**

Rincon, New Mexico, temperature overturns, semi-analytical model

# **ABSTRACT**

The Rincon geothermal system (RGS) is one of the more promising intermediate temperature (~150°C) geothermal prospects in New Mexico; one well has a bottom hole temperature of 99°C (SLH-1). This well is located about 50 m east of the East Rincon Hill Fault (ERHF) zone in the Rincon Hills in south-central New Mexico. Brackish (~ 1900 mg/l) geothermal fluids have migrated up the ERHF and flow eastwards in water-table aquifer. This blind geothermal system has no surface expression other than a series of stacked opal deposits. The temperature-depth profile measured in 1993 in SLH-1 was overturned, suggesting transient geothermal behavior. SLH-1 in 1993 had a temperature of 83.9°C just below the water table (depth of 100 m). Below the water table temperatures declined in the borehole to 70.6°C at 176-m depth before increasing. The highest temperature was 99°C at the bottom of the borehole at a depth of 371 m. We remeasured the temperature profile in SLH-1 in September 2018 and found it to be nearly unchanged in the intervening 25 years. The temperature at 100 m in 2018 was slightly warmer compared to 1993 (84.8°C) and was warmer at the minimum at 173 m (73.7°C), but otherwise the two profiles overlap perfectly. This suggests steady-state hydrothermal conditions. As a consequence of these observations, we developed and applied a semi-analytical, steady-state model describing conductive and convective heat transfer resulting from three-dimensional flow groundwater flow. The solution is based on the assumption of fault perpendicular groundwater flow (qh) within an unconfined hot water-table aguifer and regional fault-parallel flow within an underlying cooler confined aquifer (q<sub>c</sub>). Vertical conductive heat transfer is assumed to dominate above, below, and in between these stacked aguifers. The three-dimensional flow rates needed to produce temperature

overturns were evaluated using a sensitivity study. This model produces steady-state temperature overturns similar to the overturn measured in SLH-1 provided that convective heat transfer dominates within both the hot and the cooler aquifers and that  $q_b/q_c$  is about 2.

#### 1. Introduction

The Rincon geothermal system (RGS), located in the Rincon Hills along the southwest edge of the Jornada del Muerto Basin in south-central New Mexico (Figure 1), has intermediate-temperature (~150°C) reservoir potential (Witcher., 1991a, b). Pronounced groundwater elevation differences between probable upland recharge and the lowlands near the RGS (Figure 2) suggest that this is a forced convection geothermal system (Smith and Chapman, 1983). Forced convection geothermal systems are common along the Rio Grande Rift (Morgan et al., 1981; Witcher, 1988; Barroll and Reiter, 1990; Pepin et al., 2015). Temperature gradients in the recharge area in the foothills of the San Andres Mountains vary between 34 to 39.5°C/km (Figure 2B). Discharge area temperature gradients in the lowlands of the Jornada del Muerto Basin are over ten times higher (439 to 648°C/km; Figure 2C).

Temperatures measured in a slim-hole exploration well SLH-1 located about 50 m to the east of the East Rincon Hills Fault reveal a persistent 15°C temperature overturn (red and black dashed lines; Figure 2c). The first temperature-stabilized profile after core drilling of exploration well SLH-1 was collected in the RGS in 1993 (Witcher, 1998). The well SLH1 is in close proximity to the fault zone but does not cross the fault (Figure 1C). Temperature profile overturns can sometimes display anomalously high temperatures at shallow depths with cooler temperatures below. Such profiles are commonly associated with transient geothermal discharge along fault zones and lateral flow into an aquifer (Ziagos and Blackwell, 1981)

A second profile was collected in 2018 as part of this study. The linear nature of shallow temperature profiles within the vadose zone (0–70m depth) in well bores SLH-1, RAD-3 and RAD-8 also suggest steady-state conductive conditions (Figure 1c). Groundwater flow patterns, as indicated by water table contour maps, are three-dimensional (Figure 3). Elevated vertical temperature gradients closely correspond to water table elevations (Figure 3).

We hypothesize that the temperature overturn in borehole SLH-1 can be explained by a three-dimensional, steady-state groundwater flow system with components of fault parallel and perpendicular flow (Figure 4). We assume that fault-perpendicular groundwater flow  $(q_h)$  occurs within a hot water table aquifer and regional fault-parallel flow occurs within an underlying, cooler confined aquifer  $(q_c)$ . We further assume that vertical conductive heat transfer dominates above, below, and in between these stacked aquifers.

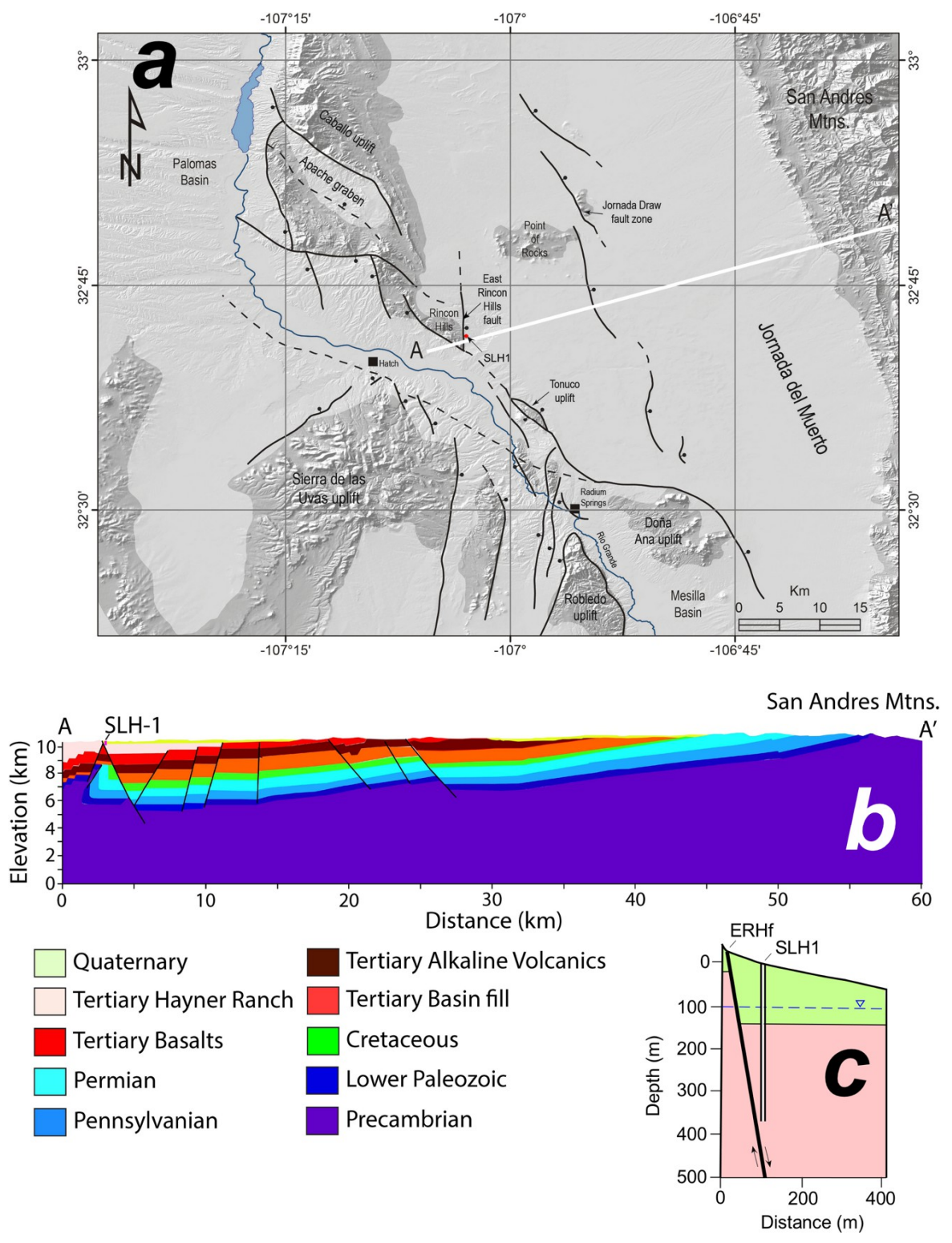


Figure 1. (a) Base map showing the location and structural setting of the Rincon Hills within the Jornada del Muerto Basin in New Mexico. (b) Idealized east-west geologic cross-section across the Jornada del Muerto Basin (A-A'). (c) Shallow, local east-west geologic cross showing the proximity of the geothermal well SLH1 to the East Rincon Hills fault (ERHf).

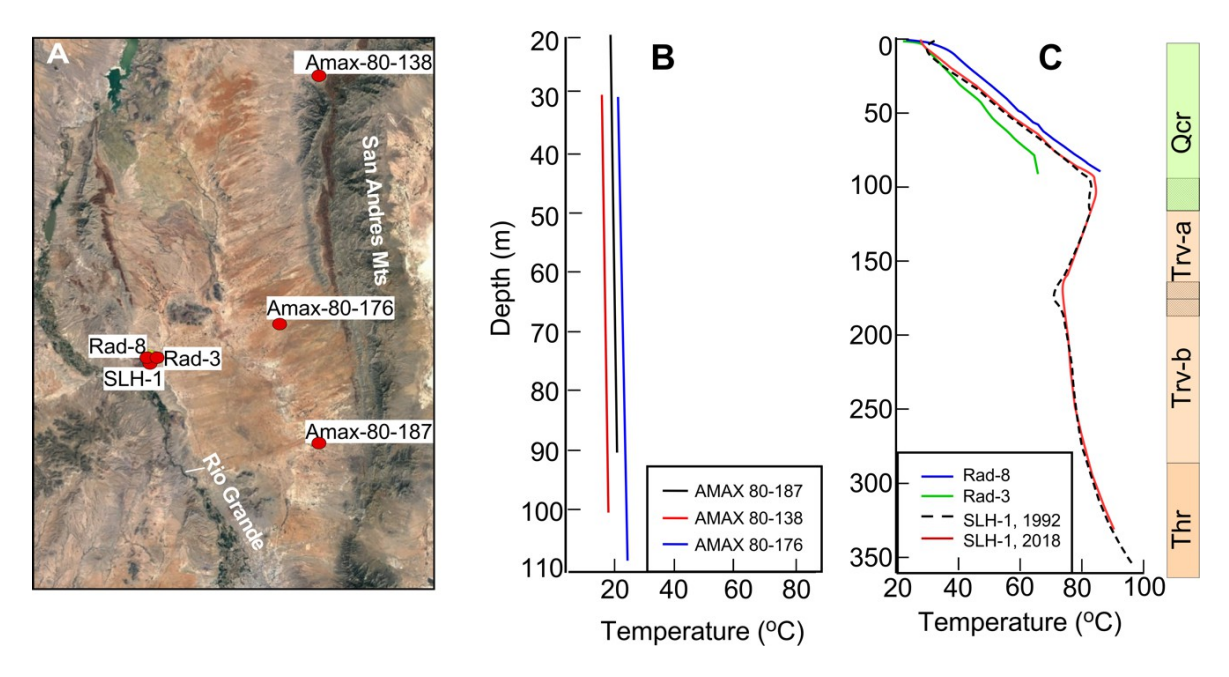


Figure 2. (A) Map showing wells near the recharge area in the San Andres Mountains and in the discharge area near the Rio Grande. (B) Upland temperature profiles on the east side of the Jornada del Muerto Basin near the recharge area. (C) Lowland wells RAD-8, RAD-3 and SLH-1 are located near a geothermal upflow zone east of the ERHF. Repeat temperature profiles were collected for well SLH-1 in 1993 and 2018. Stratigraphic column shown to the right. Thr= Hayner Ranch Formation, Trv-b and Trv-a= Rincon Valley Formation, Qcr=Camp Rice Formation (after Witcher, 1998).

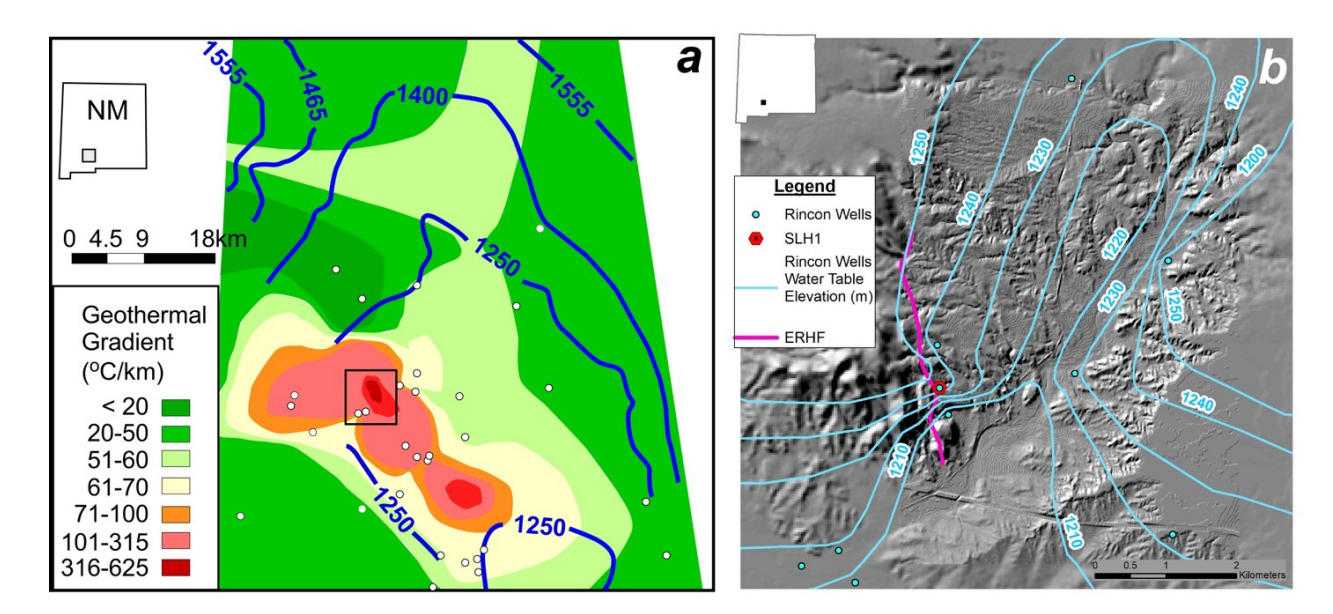


Figure 3. (a) Regional water table contour map (blue lines) across the Jornada del Muerto Basin. Green to red shaded patterns denote temperature gradients contours (°C/km). White circles denote location of temperature gradient drillholes. (b) Expanded water table contours near the East Rincon Hills Fault (ERHf purple line) near the southwest edge of the basin. Temperature gradient drillholes and water wells are indicated by the blue dots (data source James Witcher).

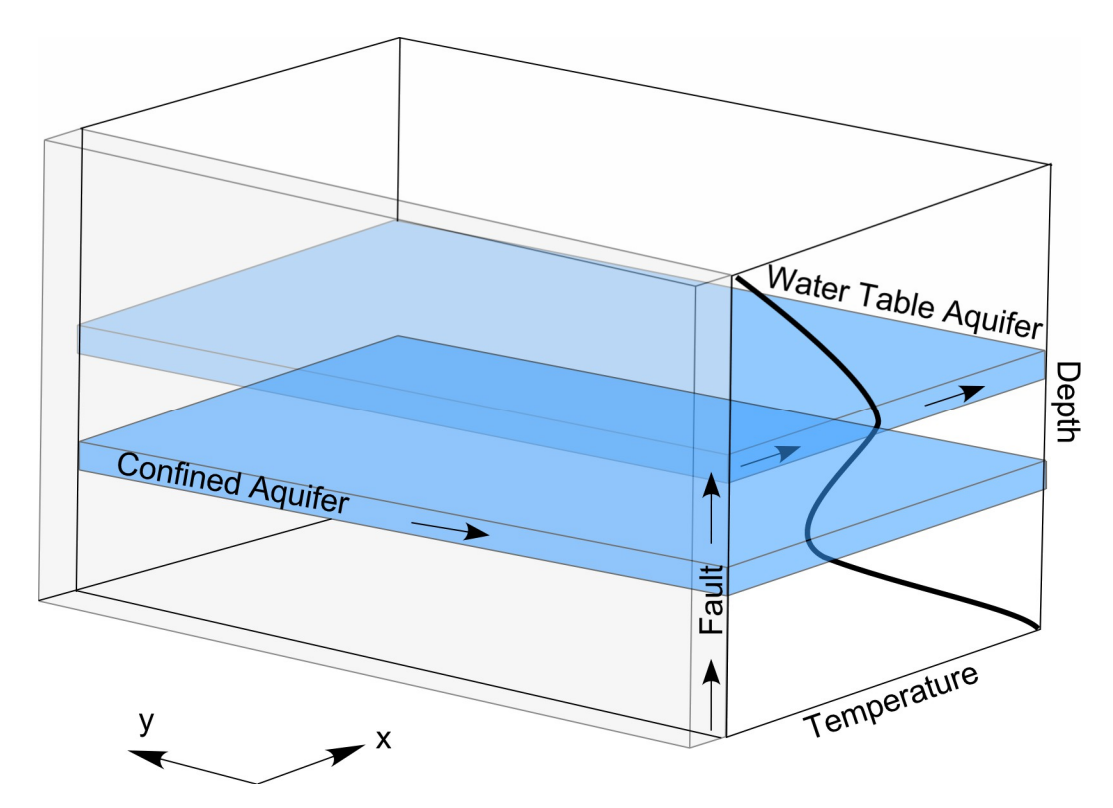


Figure 4. Conceptual model for the Rincon geothermal system.

In this study, we present a new semi-analytical solution describing conductive-convective steady-state heat transfer resulting from three-dimensional groundwater flow. We applied this semi-analytical solution in a sensitivity study to assess the three-dimensional flow rates needed to produce temperature overturns. We also fit the solution to the SLH-1 temperature profile. Our conceptual model may be applicable to other field sites with pronounced temperature inversions, such as the Beowawe geothermal system in Nevada (Howald et al., 2015).

#### 2. Geologic Setting

The Rincon geothermal system is located in the southern Rio Grande rift at the intersection of the Hatch-Rincon basin and the southern Jornada del Muerto basin (Figure 1). The Hatch-Rincon basin is a west-northwest trending half graben with master normal faults facing south to southwest (Seager and Mack, 2003). The southern Jornada del Muerto basin south of the Point of Rocks (Figure 1a) and nearest Rincon is formed by two north-striking half grabens (Seager and Mack, 1995). The East Rincon Hills Fault (ERHF; Figures 1 and 3b), facing east, forms the western half graben and hosts the upflow zone of the Rincon geothermal system. Further east, the Jornada Draw Fault (JDF) forms the eastern half graben with the hanging wall on the east. The ERHF and the JDF show Pleistocene offset. The Jornada del Muerto basin north of Point of Rocks has the regional characteristics of south-plunging syncline with the east-facing JDF and complementary half graben roughly following the basin axis (Seager and Mack, 1995; Newton et al., 2015). The east-dipping strata of the Caballo Mountains horst forms the western limb and the San Andres Mountains horst forms a stratigraphic west-dipping limb.

The Rincon geothermal system is focused in a zone of cross-cutting tectonic inversion where the north-striking ERHF footwall has uplifted and exposed sediment deposited in the west-northwest striking Hatch-Rincon half graben to form the Rincon Hills. The early rift sediments unroofed in the Rincon Hills from oldest to youngest are the Oligocene Thurman, the Miocene Hayner Ranch, and the Miocene Rincon Valley (Seager and Hawley, 1973). The Pliocene-Pleistocene Camp Rice Formation is mostly missing in the Rincon Hills; the contact between the Rincon Valley Formation and the overlying Camp Rice Formation is an angular unconformity in the Rincon area.

The units of greatest interest to this study are the Camp Rice, Rincon Valley, and the uppermost Hayner Ranch Formation. The uppermost Hayner Ranch Formation and bulk of the Rincon Valley Formation consist of distal alluvial fan and playa deposits in the Rincon Hills and in the subsurface east of the ERHF. These units dip to the south to southeast (Witcher, 1991b) and consist mostly light red-brown claystone, siltstone, fine-grained sandstone, with some gypsum. These units are aquitards and are not silicified by hydrothermal alteration. A tectonically-tilted proximal alluvial fan unit in the Rincon Valley Formation conformably overlies the Rincon Valley playa facies. This fan unit acts as an aquifer and shows pervasive silicification where it has hosted hydrothermal fluids. The Camp Rice Formation is undeformed except by fracturing and represents axial fluvial deposition of the ancestral Rio Grande. Stacks of cross-bedded fluvial channel sand, crevasse splay sands, and overbank silt and clay are typical fluvial facies (Mack et al., 2012). The Camp Rice Formation is an aquifer; but this unit maybe pervasively silicified with quartz to form quartzite where proximal flow paths of hydrothermal fluids from the ERHF traversed the unit (Witcher, 1998). Highly silicified zones of the Rincon Valley fan facies and the Camp Rice fluvial facies are both fractured (Witcher, 1998).

An important Laramide compressional basement-involved reverse fault and draping system of folds and thrusts likely provides a deep reservoir and circulation at Rincon (Witcher, 1991b and Witcher, 1998). Seager et al. (1986) describe this regional scale east- to east-northeast-vergent Laramide structure in the McLeod Hills north of Rincon that is on strike with Rincon and connects to San Diego Mountain to the south.

## 3. Rincon Geothermal System Site Description

The RGS is a "blind" system with no currently active hot springs. Summers (1976) identified a thermal water well near the intersection of the Santa Fe Railroad and Interstate 25. Later, Lohse and Schoenmackers (1985) drilled a series of shallow temperature gradient holes (TG; Figure 5) to explore for geothermal resources in northern Doña Ana County. The northernmost temperature gradient hole, TG-99, encountered a bottom hole temperature of 54.3°C at 50 m depth (Figure 5).

Seager and Hawley (1973) mapped several opal beds on both sides of the ERHF; but did not posit an origin. One of these opal beds was interpreted to have formed in cool-temperature spring-fed marshes (LeMone and Johnson, 1969). Witcher (1991a,b) recognized the potential geothermal importance of the opal beds as a possible pathfinder to a high temperature geothermal system. High temperature systems are frequently associated with opaline spring deposits, as opposed to travertine or calcium carbonate spring deposits. More recently, Mack et al. (2012) mapped the distribution and determined the chemistry of the opal beds cropping out along the Rincon Arroyo in order to test a hydrothermal-fluid origin for the opal beds at Rincon. Five continuous layers that range from 0.2 to 1 m in thickness were identified. With increasing distance from the ERHF, the opal beds transition to friable sands with opal glaebules and then to microcrystalline calcite (Figure

5). The opal beds are emplaced in the Camp Rice Formation that dates to the Pliocene and early Pleistocene (5–0.8 Ma). Strontium isotope ratios ( $^{87}$ Sr/ $^{86}$ Sr = 0.71301– 0.71724) indicate that the opal deposits precipitated from geothermal fluids that represent mixtures of water associated with deeply buried Proterozoic basement and Paleozoic carbonate rocks. The authigenic carbonate has  $\delta^{13}$ C and  $\delta^{18}$ O values consistent with a mixture of deeply derived geothermal fluids and meteoric water. The geothermal fluids that formed the opal and calcite deposits discharged as springs or resided in a near-surface water table (marsh), flowing laterally away from the ERHF (Mack et al., 2012). As the waters cooled, opal precipitated first, then calcite. The presence of opalized woody fossils (LeMone and Johnson, 1969; Seager and Hawley, 1973) suggests that the fluids discharged at the surface as springs. However, the distribution of opalized fossils is not widespread and terraced opaline spring mound terraces are not preserved. Overall, the opal beds indicate that the location of surface and near-surface discharge zone(s) varied spatially and temporally in the Rincon Hills. Each opal bed represents a paleo-spring discharge, and occurrence and preservation is likely the combined result of seismic activity on the ERHF, climate variation, and channel migration of the ancestral Rio Grande during the Pleistocene.

Witcher (1991a) mapped potential upflow zones in the RGS using radon soil-gas surveys. In the Rincon Hills, Witcher (1991a) found anomalous radon soil-gas levels (up to 322 piC/L). Subsequent drilling of thermal gradient boreholes in the Rincon area showed very high geothermal gradients within vadose zone (> 400 °C/km) (Figure 5). The gradients in RAD-8 and 4 are conductive, whereas the thermal gradients in RAD-3 and 7 decrease below the water table, indicative of an outflow plume. Self-potential (SP) surveying by Ross and Witcher (1998) provides additional information on the shape and extent of the shallow upflow zone of the RGS.

RAD-7, northeast of SHL-1, was sampled for water chemistry via airlifting (Witcher, 1991b) RAD-7 intersects the water table around 90 m depth, and has a water table temperature of 60°C. The water is predominantly a sodium-chloride fluid with a TDS of 1924 mg/L. A suite of geothermometry calculations yielded potential reservoir temperatures of 177°C (Na/K/Ca), 117°C (Na/Li), 94°C (Mg/Li), 146°C (quartz), 120°C (chalcedony), and 96°C (alpha-cristobalite). Witcher (1991b) concluded that the top of the RGS likely had temperatures 94-120°C, reflecting the range of the Na/Li, Mg/Li, chalcedony, and alpha-cristobalite geothermometer estimates. The 146°C quartz geothermometer probably reflects the minimum production reservoir temperature at depth. The Na/K/Ca geothermometer may be unreliable in where waters have flowed through carbonate rocks.

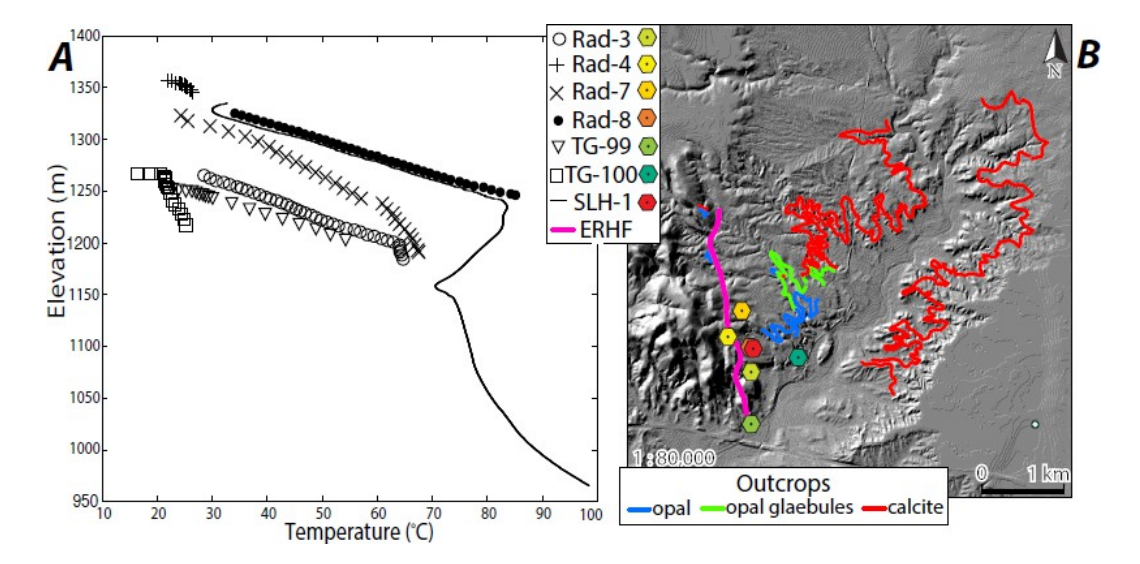


Figure 5. (A) Temperature versus elevation from Rincon temperature gradient holes drilled by Lohse and Schoenmackers (1985), Witcher (1991b), and Witcher (1998). Slope changes represent the water table.

(B) Position of opal outcrops transitioning to opal glaebules and then calcite, mapped by Mack et al. (2012). Pink line is the East Rincon Hills Fault (ERHF). Hexagon symbols are the locations of the wells that are plotted in (A).

Studies by Witcher (1991a, b) culminated in the drilling of exploration corehole SLH-1 (solid line, Figure 5; Witcher, 1998). A high-precision tool was used to measure temperatures in the well in July of 1992 after the post-drilling temperatures had mostly stabilized. The tool belonged to Sandia National Laboratory and the measurement provided a field test of a new instrument design. SLH-1 has a temperature of 81°C at the water table (92 m depth, 1,242 m elevation). The lowest temperature in the borehole is 70.6 °C at 176 m depth (1,159 m elevation) and the highest temperature is 99 °C at 371 m depth (964 m elevation) at the bottom of the borehole (Figure 4). Witcher (1998) noted significant fracturing and silicification of the units above the Rincon Valley playa facies aquitard (0-179 m depth). The 1992 temperature profile has thermal disturbances at 100 m and 179 m depth associated with zones of lost drilling fluid around high permeability fractures.

## 4. Hydrology

In the Rincon area, the shallow aquifers in the Camp Rice Formation fluvial sands, overlie the Rincon Valley Formation distal alluvial fan and playa facies aquitard. On a regional scale, groundwater in the shallow Camp Rice aquifer system originates mostly as inflow from the southeast that ultimately flows into the Hatch-Rincon Valley near Rincon (Kambhammettu et al., 2011; Wilson et al., 1981). The aquifer system is mostly recharged by San Andres, Caballo and Organ Mountain precipitation and runoff; although some recharge from the Jornada del Muerto basin floor may also occur (Hawley and Kennedy, 2004 and 2005; Ketchum, 2016; Newton et al., 2015; Rueter et al., 2021, and Wilson et al., 1981). Ephemeral flows in Rincon Arroyo provides an important local recharge source as evidenced by the best ground water chemistry quality in the region at the Village of Rincon water supply well on the east side of Rincon Arroyo (Wilson et al., 1981). This occurs despite subsurface geothermal outflow from the nearby East Rincon Hills Fault Zone to the west of the arroyo and the water well site. The decreasing elevation to the south in Rincon Arroyo provides an overall southerly flow vector and the geothermal flow has an easterly

flow as largely defined by fault orientation and contact with optimal Camp Rice aquifer permeability. Some Rincon Arroyo ephemeral flow is the result of runoff from the southern Caballo Mountains and Point of Rocks.

Overall, the Jornada del Muerto basin receives a total of 3,367 acre-feet/year (or  $4x10^6$  m³/yr) of mountain-front recharge from the Caballo, San Andres, and Organ mountains (Kambhammettu et al., 2011). The deep aquifers and flow paths occur below the Miocene Rincon Valley and Eocene Palm Park formations. Recharge is mostly from precipitation where the deep units are exposed at the surface in the Caballo and San Andres mountains (Hawley and Kennedy, 2004 and 2005; Newton et al., 2015; and Wilson et al., 1981). Groundwater travel times in the deep bedrock aquifers is slow, which allows collecting heat and chemistry.

#### 5. Methods

# 5.1. Repeat temperature measurements

In September 2018, we collected a repeat temperature profile in SLH-1 (Figure 2). The temperature logging equipment consists of a Fenwall thermistor attached to a 1 km long wireline cable that is mounted in a pickup truck covered with a camper shell. A digital multimeter attached to a computer records resistance in the thermistor and cable, which is converted to temperature by calibrating the truck-based system against a laboratory-calibrated platinum resistance thermometer. The reproducibility of the measurements is  $0.02^{\circ}$ C. This thermistor works best in water. Measurements in the field are taken at 1 m intervals, and the cable is lowered down the well at a rate of 2 m/min. Vertical geothermal gradients,  $\Delta T/\Delta z$ , are estimated by linear regression using least squares estimation.

#### 5.2 Hydrothermal model

We developed a steady-state, semi-analytical solution that captures the essential features of the Rincon geothermal system upflow zone. The groundwater flow system consists of an upper and lower aquifer separated by a confining unit, with additional confining layers above and below the aquifers (Figure 4). We assume purely convective heat transport dominates within the two aquifers. In addition, conductive heat transport dominates within all confining units. Flow in the upper water table aquifer results from hydrothermal discharge issuing from a fault conduit (Figure 4). The maximum temperature ( $T_h$ ) in the water table aquifer occurs along the fault zone at (x,0). Flow in the upper aquifer system is in the x-direction. The lower confined aquifer system has flow prescribed in the y-direction and is at a right angle to the upper aquifer flow system. The background aquifer temperature ( $T_c$ ) that enters the confined aquifer upstream provides a source of relatively cool fluids that can maintain a thermal overturn. Temperatures within the water table aquifer are denoted by  $T^h(x,y)$ . The fault is located along the line segment (0,y) (Figure S1). Temperatures within the lower confined aquifer zone are denoted by  $T^c(x,y)$ . Cooler background temperatures enter the confined aquifer along the line segment (x,0).

Analytical solutions are obtained along two of the boundaries of the model domain because the specified temperature conditions  $T_c$  and  $T_h$  reduce the number of unknowns. That is, along the boundary where  $T^!$  is fixed at  $T_h$  in the upper aquifer along the line segment (0,y), an analytical solution in the lower aquifer can be obtained for  $T^*$  along this same line segment. Alternatively, along the line segment (x, 0) within the confined aquifer where the temperature is fixed  $T^*$ , an

analytical solution can be found in the upper aquifer for  $T^!$ . The two analytical solutions are given by:

$$T^{!}(x,0) = \frac{-1!}{n} + T! - \frac{-1!}{n} + exp[C \# x]$$
 (1a)

$$T^{\$}(0, y) = T_{!} + C_{\%}[T_{\$} - T_{!} - C_{\%}]exp[-C_{\&}x]$$
(1b)

where C<sub>1</sub>-C<sub>5</sub> are constants and are defined in the supplemental materials section.

For the interior of the model domain both  $T^h$  and  $T^c$  are dependent variables and appear in both aquifer equations. The governing conductive-convective heat transfer equations we numerically solved are given by:

where  $T_1$  is the computed interior steady-state temperatures of the model domain,  $D_1 - D_5$  and  $E_1$  are constants defined in the supplemental materials section. We used the analytical solution from equation (1a) to specify  $T^h$  along the line segment (x,0) in the upper aquifers and the analytical solution (1b) to specify  $T^c$  along the line segment (0,y) in the lower aquifer. We applied a constant temperature boundary  $T_h$  along (0,y) in the upper aquifer and  $T_c$  along (x,0) in the confined aquifer. All other boundaries were specified as no flux conditions. We used an upwinding scheme to eliminate numerical oscillations for the convective terms. See the supplemental materials section for the full derivation of the analytical solutions and numerical approximations. The semi-analytical solution is available as a MATLAB code.

#### 6. Results

# 6.1. Comparison of 1992 and 2018 temperature profiles

The temperature profiles collected in 1992 and 2018 SLH-1 (Fig. 2c; red and black dashed lines) are nearly identical. There appears to be about 2°C temperature change at the inflection points at 100 m and 180 m depth. This may be because the drilling fluids cooled the rocks outside the well annulus and the thermal regime had not fully equilibrated when the first temperature profile was collected. The small difference in temperatures between the two temperature profiles measurements supports our hypothesis of steady-state conditions.

# 6.2. Semi-Analytical model results

We ran a sensitivity study in which we varied the groundwater fluxes  $q_h$  and  $q_c$  within the water table and confined aquifer (Table 1). Thermal properties, basal heat flow, and porosity were fixed (Table 2). The values chosen in Table 2 represent normal heat flow conditions within the continental crust. We used a grid of 402 nodes in both the x and y-directions with a fixed  $\Delta x$  and  $\Delta y$  of 0.25 m. The solution domain was 100 m x 100 m.

**Table 1**. Variable parameters used in sensitivity study and SLH-1 model run.

	qh	qc	Peh	Pec	$q_h/q_c$			
Scenario	(m/yr)	(m/yr)						
1	0.79	0.00079	5.2	0.005	1000			
2	7.9	0.79	52	5.2	10			
3	7.9	0.39	52	2.6	20			
4	7.9	1.57	52	26	2			
SLH-1	22	19	142	125	2			

**Table 2.** Fixed parameters used in sensitivity study.

			Δx,	Ts ∆y	$T_h$	Te		k <sub>1</sub> -k <sub>5</sub>
φ	Nx	$N_y$	(m)	(°C)	(°C)	(°C)	$J_{z}\left(W/m^{2}\right)$	(W/ m · °C)
0.25	402	402	0.25	10	100	12.2	0.06	2
Z!	<b>Z</b> "	<b>Z</b> #	<b>Z</b> #	ho\$	<b>C</b> \$			
(m)	(m)	(m)	(m)	(m)	(J/kg/°C)			
0	100	150	300	1000	4180	_		

We used two thermal Peclet (Pe) numbers to characterize the ratio of convection to conduction in this study:

where Pe<sub>h</sub> and Pe<sub>c</sub> are the thermal Peclet numbers for the hot and cold reservoirs and L is the model domain length (100m).

The sensitivity study included four runs. Run 1 can be characterized as having relatively low thermal Peclet numbers of 0.79 and 0.00079 for the hot and cold aquifers, respectively. The flow rate within the upper aquifer was set to be 1000 times greater than that of the lower aquifer in this scenario. Inspection of the temperature profiles moving away from origin suggests that convective heat transport in the confined aquifer was too low to create a temperature overturn (Figure 6a-6e). They are comparable in form to the solution of Ziagos and Blackwell (1986). For Run 2,  $q_h$  was increased by a factor of 10 and  $q_c$  is increased by a factor of 1000 so that convection dominates in both aquifer systems (i.e.  $Pe_2$  and  $Pe_4$  were 52 and 5.2, respectively; Table 1). A temperature

overturn is apparent out to about 7 m from the origin (Figure 6f-6g). In Run 3, qh remained unchanged and qc was decreased by a factor of 10 resulting in a 20-fold difference in Darcy flux between the upper and lower aquifers. Here the temperature overturn is confined to 6 m from the origin (Figure 6k-6o). In Run 4, there was only a factor of 2 difference between the Darcy flux within the upper and lower aquifers (Figure 6p-6t). Like Run 2, an overturn can be seen across the 100 m x 100 m domain. The grid thermal Peclet numbers were relatively high; 52 and 26, respectively for the water table and confined aquifers. A plot of the two analytical solutions for Run 4 of our sensitivity study is presented in Figure S2 in the supplemental materials section. The three-dimensional nature of the convective temperature anomalies can be seen in plane view temperature contour maps presented in Figures S3-S4 for the sensitivity study.

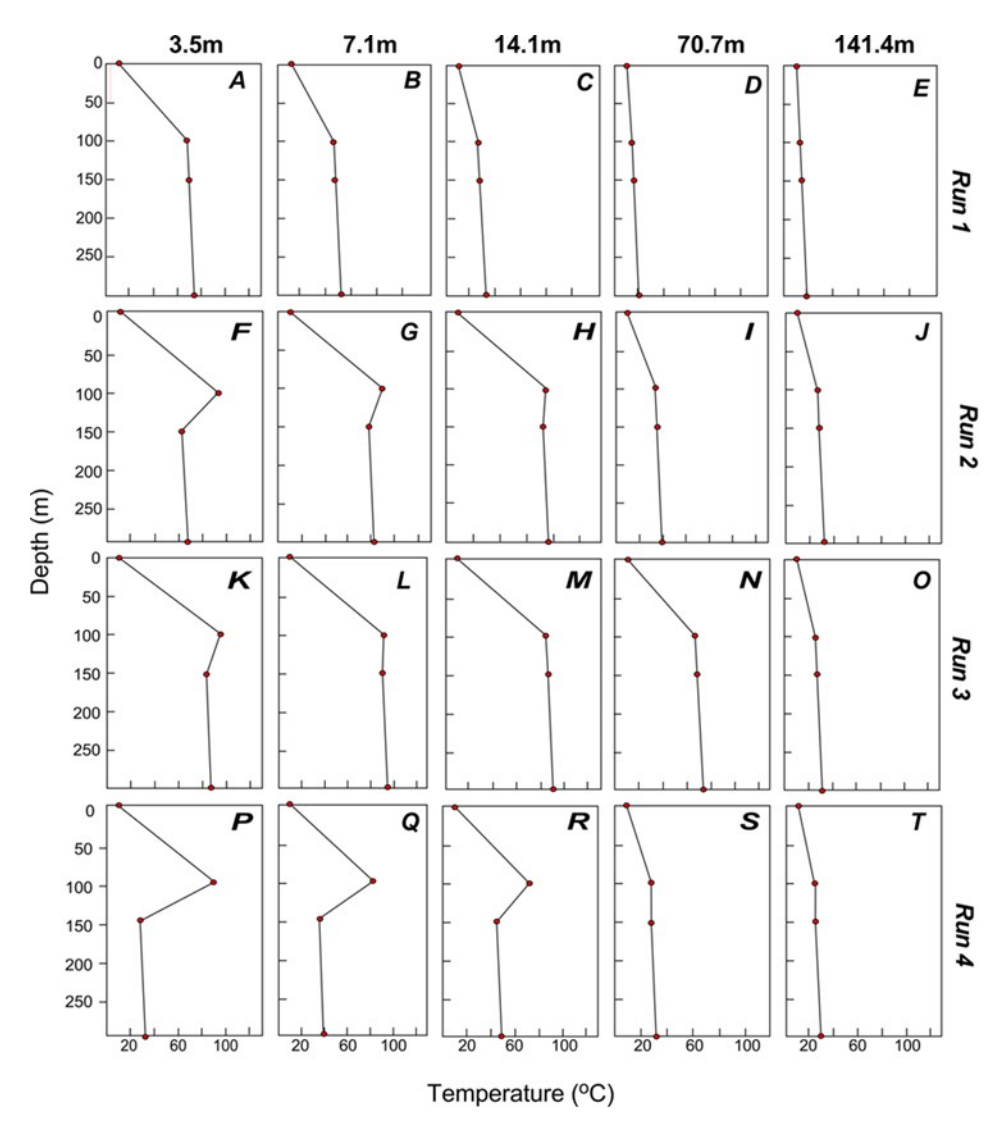


Figure 6. Temperature versus depth for select locations from sensitivity study. See Table 1 for values of parameters used in semi-analytical solutions. The locations of profiles 3 m, 6 m, 12.5 m, 50 m, and 100 m are located along a line oriented 45° from the horizontal axis measured from the origin.

#### 6.3 SLH-1 Model

The temperature overturn in the Rincon well SLH-1 is mostly reproduced using our analytical solution (Figure 7). This required assigning an elevated basal heat flow of  $200 \text{ mW/m}^2$  and aquifer flow rate of about 22 and 19 m/yr within the unconfined and confined aquifers, respectively (Table 1). Due to quartz silicification of the sediments, we assumed a porosity of 0.1. Contour plots of the unconfined and confined aquifers indicate a highly three-dimensional thermal regime (Fig. 7b, 7c). The best fit match to the SLH-1 well was found at x = 50 m, y = 100 m.

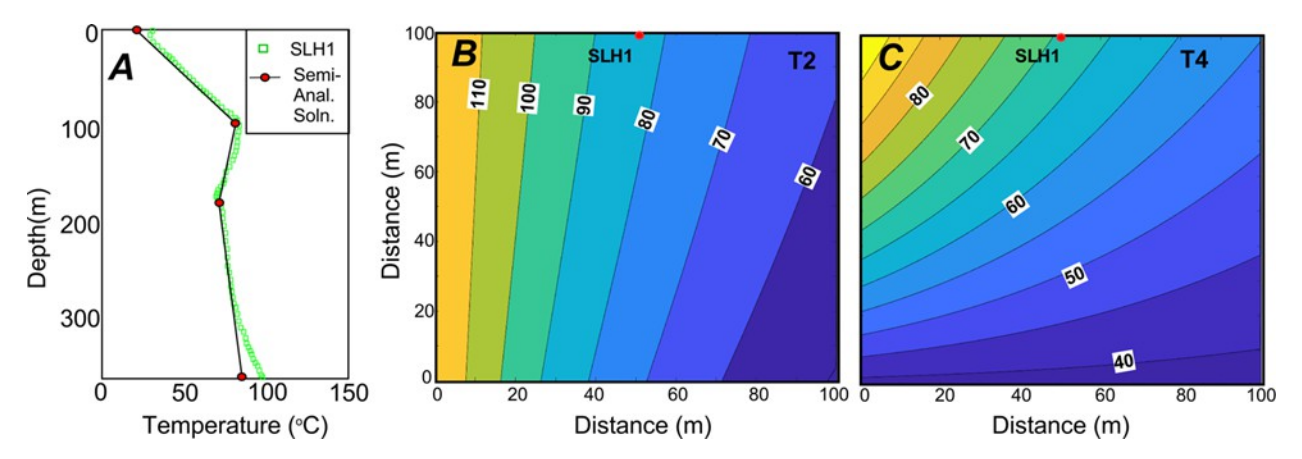


Figure 7. (A) Best fit analytical model to SHL-1 Rincon well. (B) Map view showing temperature contours in the upper aquifer (T2). (C) Map view showing temperature contours in the lower aquifer (T4).

# 7. Discussion

The regional north-south hydraulic gradient near the ERHF is about 0.08. Using the flux estimates from our analytical solution  $(22\text{m/yr} \text{ or } 7\text{x}10^{-7} \text{ m/s})$  yields a hydraulic conductivity of about  $9 \cdot 10^{-6}$  m/s or a permeability of about  $9 \cdot 10^{-13}$  m<sup>2</sup>. This is on the order of a permeable sand aquifer (Freeze and Cherry, 1979). Since the sedimentary units near the ERHF are highly cemented, bulk permeability is likely related for fracture spacing and aperture. Using Snow's law estimate of permeability:

$$k = \frac{\dot{s}}{\sharp + \dot{s}} \tag{4}$$

where k is permeability, s is fracture spacing, and b is the fracture aperture. A fracture aperture of 0.1 mm and a spacing of 10 cm would yield a bulk permeability of about  $8 \cdot 10^{-13}$  m<sup>2</sup>.

Ge (1998) developed a steady-state analytical solution for borehole convective temperature anomalies. She demonstrated that steady-state temperature overturns can result from subhorizontal flow along interconnected fracture sets. Her analytical solution predicts a return to conductive conditions below the fracture rock outflow zone. The solution is clearly applicable to temperature overturns within a unidirectional flow system. In SLH-1, there are three linear temperature segments from 0–100 m, 100–180 m, and 180–280 m. All have different slopes (Fig. 5a). The linear nature of these segments argues for steady-state conditions. Below 280 m depth there is some curvature in the temperature-depth profile that may result from a trend of increasing porosity and decreasing thermal conductivity perhaps due to the absence of hydrothermal mineralization.

We estimate the total opal endowment at Rincon is about 6.8 x 10<sup>8</sup> kg (Horne, 2019). This would yield an average silica endowment of about 1.3x10<sup>8</sup> kg per bed. A chemical analysis for the exploration well RAD-7 indicated a dissolved silica concentration of 116.7 mg/L. Using the flux our SLH-1 model of about 22 m/yr, it would only take 1280 years to deposit this amount of opal, assuming 100% efficiency of silica precipitation. This suggests that silica kinetics must play an important role in reducing the rate of silica precipitation (Rimstidt and Barnes, 1980, Rimstidt and Cole, 1983).

#### 8. Conclusions

Repeat temperature measurements were made in a geothermal exploration well located about 50 m east of the north-south trending ERHF zone within the Jornada del Muerto Basin, New Mexico. Temperatures in this well (SLH-1) did not change over a period of 25 years. The well displays a prominent temperature inversion of 15°C over a vertical distance of about 60 m. The persistence of the temperature profile suggests steady-state conditions. Groundwater flow directions, as indicated by water table contour maps indicate flow is highly three-dimensional (Figure 3). We used a new semi-analytical solution to demonstrate that the temperature overturn observed in borehole SLH-1 can result from a multi-level, three-dimensional, conductive/convective fluid flow system. We also applied this solution in a sensitivity study. We found that flow rates within the upper hot water table aquifer and the cooler confined aquifer had to be relatively high (~ 8 m/yr) and less than or equal to one order of magnitude of one another in order to sustain thermal inversions away from the fault zone.

# Acknowledgement

Funding for this research was provided by the National Science Foundation (EAR1830172).

## REFERENCES

- Barroll, M.W. and Reiter, M. "Analysis of the Socorro Hydrogeothermal System: Central New Mexico." *Journal of Geophysical Research: Solid Earth*, 95, (1990), 21949-21963. https://doi.org/10.1029/JB095iB13p21949
- Freeze, R. A. and Cherry, J. A. "Groundwater." Prentice-Hall, Inc., Englewood Cliffs, NJ, (1979) 604 p.
- Ge, S., "Estimation of Groundwater Velocity in Localized Fracture Zones from Well Temperature Profiles." *Journal of Volcanology and Geothermal Research*, 84, (1998), 93-101. <a href="https://doi.org/10.1016/S0377-0273(98)00032-8">https://doi.org/10.1016/S0377-0273(98)00032-8</a>
- Hawley, J.W., and Kennedy, J.F., "Creation of a Digital Hydrogeologic Framework Model of the Mesilla Basin and Southern Jornada del Muerto Basin." N. M. Water Resources Research Institute, New Mexico State University; prepared for Lower Rio Grande Water Users Organization; *Technical Completion Report*, 332, (2004), 105 p.
- Hawley, J.W., Kennedy, J.F., Ortiz, M.A., and Carrasco, S., "Creation of a Digital Hydrogeologic Framework Model of the Rincon Valley and Adjacent Areas of Dona Ana, Sierra And Luna

- Counties NM." N.M. Water Resources Research Institute, New Mexico State University; *Addendum to Technical Completion Report 332*, (2005) on CD ROM.
- Horne, M., "Assessing the Rincon Geothermal System using Transient Electromagnetic Surveys and Hydrothermal Modeling." MSc Thesis, New Mexico Institute of Mining and Technology, (2019), 107 p.
- Howald, T., Person, M., Campbell, A., Lueth, V., Hofstra, A., Sweetkind, D., Gable, C.W., Banerjee, A., Luijendijk, E., Crossey, L. and Karlstrom, K., "Evidence for Long Timescale (> 10<sup>3</sup> Years) Changes in Hydrothermal Activity Induced by Seismic Events." *Geofluids*, 15, (2015), 252-268. https://doi.org/10.1111/gfl.12113
- Kambhammettu, B.V.N.P., Allena, P., and King, J.P., "Simulation of Groundwater Flow in the Southern Jornada Del Muerto Basin, Doña Ana County, New Mexico." N. M. Water Resources Research Institute-NMSU, *Technical Completion Report 352, prepared for Lower Rio Grande Water Users Organization (LRGWUO)*, (2010), 63 p.
- Ketchum, D. G., High-Resolution Estimation of Groundwater Recharge for the Entire State of New Mexico Using a Soil-Water-Balance Model." MSc Thesis, New Mexico Institute of Mining and Technology (2016).
- LeMone, D.V., and Johnson, R.R., "Neogene Flora from the Rincon Hills, Doña Ana County, New Mexico." *New Mexico Bureau of Mines and Mineral Resources Circular*, 104, (1969) 77-88.
- Lohse, R.L. and Schoenmackers, R., "Geothermal low-temperature reservoir assessment in northern Dona Ana County, New Mexico.", New Mexico Energy Research and Development Institute Report NMERDI-2-71-4220, (1985), 150 p.
- Mack, G. H., Jones, M. C., Tabor, N. J., Ramos, F. C., Scott, S. R., and Witcher, J. C. "Mixed Geothermal and Shallow Meteoric Origin of Opal and Calcite Beds in Pliocene-Lower Pleistocene Axial-Fluvial Strata, Southern Rio Grande Rift, Rincon Hills, New Mexico, U.S.A." *Journal of Sedimentary Research*, 82, (2012), 616–631. <a href="https://doi.org/10.2110/jsr.2012.55">https://doi.org/10.2110/jsr.2012.55</a>
- Morgan, P., Harder, V., Swanberg, C. A., and Daggett, P. H., "A Ground Water Convection Model for Rio Grande Rift Geothermal Resources." *Transactions, Geothermal Resources Council*, 5, (1981), 193-196.
- Newton, T., Kludt, T., Love, D., and Mamer, E., "Hydrogeology of Central Jornada Del Muerto: Implications for Travel Along El Camino Real de Tierra Adentro, Sierra And Doña Ana Counties, New Mexico." *New Mexico Bureau of Geology and Mineral Resources Open-File Report*, 573, (2015), 55 p.
- Pepin, J.D., Person, M., Phillips, F., Kelley, S., Timmons, S., Owens, L., Witcher, J. and Gable, C.W., "Deep fluid circulation within crystalline basement rocks and the role of hydrologic windows in the formation of the Truth or Consequences, New Mexico low-temperature geothermal system". *Crustal Permeability*, (2012), p.155-173.
- Rimstidt, J.D. and Barnes, H.L., "The Kinetics of Silica-Water Reactions." *Geochimica et Cosmochimica Acta*, 44, (1980), 1683–1699. <a href="https://doi.org/10.1016/0016-7037(80)90220-3">https://doi.org/10.1016/0016-7037(80)90220-3</a>

- Rimstidt, J.D. and Cole, D.R., "Geothermal Mineralization I: The Mechanism of Formation of the Beowawe, Nevada, Siliceous Sinter Deposit." *American Journal of Science*, 283, (1983), 861-875.
- Ross, H. P. and Witcher, J. C., "Self-Potential Surveys of Three Geothermal Areas in the Southern Rio Grande Rift, New Mexico." *New Mexico Geological Society, Guidebook 49*, (1998), 93-100.
- Rueter, S., Cadol, D., Phillips, F. M., and Newton, B. T., "Evaluating Focused Aquifer Recharge in the Jornada Experimental Range, NM, Using Chloride Profile Analysis." New Mexico Water Resources Research Institute, New Mexico State University, *Technical Completion Report* 392, (2021),36 p.
- Seager, W. R., Mack, G. H., Raimonde, M. S., and Ryan, R. G., "Laramide Basement-Cored Uplift and Basins in South-Central New Mexico." New Mexico Geological Society, Guidebook 37, (1986), 123-130.
- Seager, W. R. and Mack, G. H., "Jornada Draw Fault: A Major Pliocene-Pleistocene Normal Fault in the Southern Jornada del Muerto." *New Mexico Geology*, 17, (1995), 37-43.
- Seager, W. R. and Mack, G. H., "Geology of the Caballo Mountains, New Mexico." *New Mexico Bureau of Geology and Mineral Resources Memoir*, 49, (2003), 136 p.
- Seager, W. R. and Hawley, J. W., "Geology of Rincon Quadrangle, New Mexico." *New Mexico Bureau of Mines and Mineral Resources Bulletin*, 101, (1973), 1–50.
- Smith, L. and Chapman, D.S., "On the Thermal Effects of Groundwater Flow: 1. Regional Scale Systems." *Journal of Geophysical Research: Solid Earth*, 88, (1983), 593-608. https://doi.org/10.1029/JB088iB01p00593
- Summers, W. K., "Catalogue of Thermal Waters in New Mexico." *New Mexico: Bureau of Mines and Mineral Resources Hydrologic Report* 4, (1976), 80 p.
- Wilson, C. A., White, R. R., Orr, B. R. and Roybal, R. G., "Water Resources of the Rincon and Mesilla Valleys and Adjacent Areas, New Mexico." *New Mexico State Engineer Technical Report* 43, (1981), 514 p.
- Witcher, J. C., "Geothermal Resources of Southwestern New Mexico and Southeastern Arizona." *New Mexico Geological Society, Guidebook 39*, (1988), 191-197.
- Witcher, J. C., "Radon Soil-Gas Surveys with Diffusion-Model Corrections in Geothermal Exploration." Transactions, Geothermal Resources Council, 15, (1991a), 301–308.
- Witcher, J. C. "The Rincon Geothermal System, Southern Rio Grande Rift, New Mexico: A Preliminary Report on a Recent Discovery." *Transactions, Geothermal Resources Council*, 15, (1991b), 202–212.
- Witcher, J.C., "A Geothermal Resource Database, New Mexico." Southwest Technology Development Institute, New Mexico State University, (1995), 32 p., 6 appendices.
- Witcher, J.C., "The Rincon SLH1 geothermal well." New Mexico Geological Society, Guidebook 49, (1998), 35-38.

Ziagos, J.P. and Blackwell, D.D., "A Model for the Transient Temperature Effects of Horizontal Fluid Flow in Geothermal Systems." *Journal of Volcanology and Geothermal Research*, 27, (1986), 371-397. <a href="https://doi.org/10.1016/0377-0273(86)90021-1">https://doi.org/10.1016/0377-0273(86)90021-1</a>

# **Supplemental Materials**

# S1. Transport Equations

Our semi-analytical solution considers an idealized steady-state, three-dimensional flow system depicted in Figure 4 and S1. The upper (water table) flow system results from hydrothermal discharge issuing from a deep permeable fault zone. A lower confined aquifer system with flow parallel to the fault zone and at a right angle to the upper aquifer flow system provides a source of relatively cool water that sustains the thermal overturn at late time (Figure S1). Temperatures within the water table aquifer hosting a geothermal outflow zone issuing from the fault are denoted by  $T^h(x,y,z_h)$ . The depth of the unconfined aquifer is denoted by  $z_h$ . Flow is solely in the x-direction within the water table aquifer. Temperatures within the lower, relatively cool confined aquifer zone are denoted by  $T^c(x,y,z_c)$ . The depth of the confined aquifer is denoted by  $z_c$ . Flow is solely in the y-direction within the confined aquifer.

There are five temperature regimes in our model:

$$T^4(x, y, z), 0 \le z < z_1$$
 (1a)

$$T^{!}(x,y), z = z_{!} \tag{1b}$$

$$T^{5}(x,y,z), z_{!} < z < z_{\$} \tag{1c}$$

$$T^{\$}(x,y), z = z_{\$} \tag{1d}$$

$$T^{6}(x, y, z), z_{5} < z \le z_{3}$$
 (1e)

where  $T^*$ ,  $T^*$ , and  $T^{\%}$  are the conductive temperatures in the three confining unit layers 1 (upper), 3 (middle), and 5 (lower) and  $z_b$  is the depth to the bottom of the model domain (Figure S1). At the boundaries of each confining layer, we enforce the following conditions:

$$T^4(x, y, 0) = T. \tag{2a}$$

$$T^{4}(x, y, z_{1}) = T^{!}(x, y)$$
 (2b)

$$T^{5}(x, y, z_{1}) = T^{1}(x, y)$$
 (2c)

$$T^{5}(x, y, z_{5}) = T^{5}(x, y)$$
 (2d)

$$T^{6}(x, y, z_{3}) = T^{\$}(x, y) + \frac{7}{2}(z_{3} - z_{\$})$$
(2e)

where  $J_z$  is the basal heat flux and  $\lambda$ . is the thermal conductivity of the lowest layer. For the aquifer, we specify the following constant value boundary conditions:

$$T^!(0,y) = T_! \tag{3a}$$

$$T^{\$}(x,0) = T_{\$} \tag{3b}$$

where  $T_h$  and  $T_c$  are the specified temperatures along the edges of the two aquifers. Boundaries not covered by the analytical solution were set to no flux conditions:

$$\frac{1}{1}\frac{1}{1}\frac{1}{1}\frac{1}{1}\frac{1}{1} = 0$$
 (4a)

$$\frac{1}{1}\frac{(1)^{\$}(1/2+1)}{1+1} = 0 \qquad \frac{1}{1}\frac{(1+1)^{\$}}{1+1} = 0 \tag{4b}$$

We imposed a specified temperature boundary condition at analytical solutions on two additional boundaries described below. The steady-state solution is linear in z for T<sup>u</sup>, T<sup>m</sup>, and T<sup>l</sup>:

$$T^{4}(x,y,z) = T_{-} + - (T^{1}(x,y) - T_{-})$$
(5a)

$$T^{5}(x,y,z) = \frac{...*}{.#;.*} T^{1}(x,y) + \frac{...#}{.*;.#} T^{*}(x,y)$$
(5b)

$$T^{6}(x,y,z) = T^{\$}(x,y) + \frac{7}{2}(z-z_{\$})$$
 (5c)

In the aquifers, conservation of heat gives rise to the following energy balance equation in the upper and lower aquifers:

$$-\lambda \stackrel{\frown}{\rightarrow} + \lambda \stackrel{\frown}{=} = a \ q \stackrel{\frown}{\rightarrow}^{\#}$$

$$(6a)$$

$$-\lambda \cdot \gamma \cdot + \lambda \frac{\gamma}{} = a \ q \ \gamma \cdot \frac{\gamma}{}$$

$$(6b)$$

where  $\lambda(, \lambda)$ , and  $\lambda$  are the thermal conductivities in the three confining units,  $a_2$  is  $\rho * c * b +$ ,  $a_1$  is  $\rho * c * b_1$ ,  $q_1$  is the Darcy flux in the x-direction in the hot layer 2,  $q_1$  is the Darcy flux in the y-direction in the cold layer 4, and  $b_2$  and  $b_4$  are the respective thicknesses of layers 2 and 4. Substituting equations 5a - 5c into equations 6a and 6b yields:

$$-\lambda )^{\#(*,0)} + )^{\$(*,0)} + + J = a \ q \ \underline{)^{\&}}$$

$$-\#(*,0) = -3 + J = a \ q \ \underline{)^{\&}}$$

$$-\#(*,0) = -3 + J = a \ q \ \underline{)^{\&}}$$

$$-\#(*,0) = -3 + J = a \ q \ \underline{)^{\&}}$$

$$-\#(*,0) = -3 + J = a \ q \ \underline{)^{\&}}$$

$$-\#(*,0) = -3 + J = a \ q \ \underline{)^{\&}}$$

$$-\#(*,0) = -3 + J = a \ q \ \underline{)^{\&}}$$

$$-\#(*,0) = -3 + J = a \ q \ \underline{)^{\&}}$$

$$-\#(*,0) = -3 + J = a \ q \ \underline{)^{\&}}$$

or

$$\frac{')^{\$(*,()}}{=} = \frac{\#}{2} \underbrace{-2 \cdot + T!(x,y) - \#}_{-\$ \cdot \$} \underbrace{-2 \cdot + T\$(x,y) + 7(}_{-\$ \cdot \$ \cdot \$} \underbrace{-3 \cdot \$ \cdot \#}_{-\$ \cdot \$ \cdot \#} \underbrace{-3 \cdot \$ \cdot \#}_{-\$ \cdot \$ \cdot \#} \underbrace{-3 \cdot \$ \cdot \#}_{-\$ \cdot \$ \cdot \#} \underbrace{-3 \cdot \$ \cdot \#}_{-\$ \cdot \$ \cdot \$} \underbrace{-3 \cdot \$ \cdot \#}_{-\$ \cdot \$} \underbrace{-3 \cdot \$}_{-\$ \cdot \$} \underbrace{-3 \cdot \$ \cdot \#}_{-\$ \cdot \$} \underbrace{-3 \cdot \$}_{-\$ \cdot \$} \underbrace{-3 \cdot \$}_{-\$ \cdot \$}_{-\$ \cdot \$} \underbrace{-3 \cdot \$}_{-\$ \cdot \$}_{-\$ \cdot \$} \underbrace{-3 \cdot \$}_{-\$ \cdot \$}_{-\$ \cdot \$} \underbrace{-3 \cdot \$}_{-\$ \cdot \$}_{-\$ \cdot$$

# S2. Analytical Solution along Boundaries of Solution Domain

Far from the origin (0,0), equations 7a and 7b have a constant solution of:

$$T' = \frac{\log_2 > 7_{c_{\#}}}{2!}$$
= 2<sub>1</sub>

$$T^{\$} = \frac{0.02.2 \ge 2.7 (.\$:7.(.\$:2) \ge 2.?_{1.\$}}{2.8}$$
(8b)

Person et al.

If we let T'(x,y) = T' + T'(x,y) and T''(x,y) = T'' - T''(x,y) (since we expect T' to be cooling off and T<sup>"</sup> to be warming), we get:

$$-\lambda_{\#} \frac{1}{!} - \lambda_{,} \frac{1}{!} \frac{1}{!} \frac{1}{!} + a_{+}q_{!} \frac{1}{!} \frac{1}{!}$$

$$\frac{1}{!} \frac{1}{!} \frac{1}$$

$$-\lambda_{\#} \frac{)_{!}^{\#}}{.} - \lambda_{,} \frac{)_{!}^{\#}(*,O) > !}{!} (*,O) + = a_{+}q! \frac{)^{\#}}{!}$$

$$-\lambda_{,} \frac{)_{!}^{\#}(*,O) > !}{!} (*,O) + = a_{\%}qs \frac{)^{\$}}{!}$$

$$-\lambda_{,} \frac{)_{!}^{\#}(*,O) > !}{!} (*,O) + = a_{\%}qs \frac{)^{\$}}{!}$$

$$(9a)$$

$$(9b)$$

where all parameters are positive and  $z_c > z_h$ . These equations have the form:

$$\sum_{t*}^{t} = -AT^{t} - BT^{s} \tag{10a}$$

$$\frac{D!}{C} = -CT^{\$} - CT!$$
(10b)

with A, B, and C > 0. Looking first for a solution in the form of the exponential of a linear function of x and y, we find that for real r, and any function of r, k(r), there is a solution of the form:

$$T_{\#}! = k(r)e^{;(@>AB)*;\frac{n^{23!}}{2}}$$

$$(11a)$$

$$(11a)$$

$$T_{\#} = rk(r)e 2 (11b)$$

Thus

$$T_{\#}! = \int k(r)e^{:(@>AB)^*;\frac{n^{23!}}{2}(} dr$$
 (12a)

$$T_{\#}^{\$} = \int rk(r)e^{;(@>AB)^{*};\frac{n^{23}!}{2}} dr$$
 (12b)

As x or y gets large, these approach zero and our solutions approach  $T^{!}$ ,  $T^{"}$  as given in equation

(8). Using all the relevant variables defined above, the two analytical solutions along the boundaries (x,0) for T<sup>h</sup> and (0,y) for T<sup>c</sup>, we arrive at the analytical solutions within the upper and lower aquifers:

$$T^{!}(x,0) = \frac{-1}{x} + T^{!} - \frac{-1}{x} + \exp[C \pi x]$$
(13a)

$$T^{\$}(0, \gamma) = T_{!} + C_{\%}[T_{\$} - T_{!} - C_{\%}]exp[C_{\&X}]$$
(13b)

where  $C_1$ - $C_5$  are given by:

$$C = \frac{\lambda . T_{\$}}{L} + \frac{\lambda \#}{L}$$

$$C = \frac{\lambda \# T_{\$}}{L} + \frac{\lambda L}{L}$$

$$C = -\frac{\lambda \#}{L}$$

$$C_{\%} = \frac{I_{3}(z_{\$} - z_{!})}{\lambda_{*}}$$

$$C_{\&} = \frac{\lambda_{*}}{[(z_{!} + k_{*})(z_{\$} - z_{!}) a_{\%} V q_{\$}]}$$

#### S3. Governing Transport Equations in the Aquifers

We can solve the first equation 7c for  $T^c$  and substitute this into equation 7d, giving us:

where

$$\frac{=\frac{\lambda T_{\$}}{(z_{\$}-z_{!})a_{\%}q_{\$}}$$

$$D_{+} = \frac{(\lambda \# - \lambda)\lambda \#}{\frac{+ \lambda \# Z\$}{(Z\$ - Z!)a\%q\$}}$$

$$D, \quad \frac{=}{\frac{\lambda \lambda}{\frac{z_!(z_* - z_!)a_+q_!a_*q}{\$}}}$$

$$D_{\%} = \frac{\lambda \lambda \#}{z_!(z_{\$} - z_!)a_+q_!a_{\%}q_{\$}}$$
 
$$D_{\&} = \frac{\lambda}{a_{\%}q_{\$}(z_{\$} - z_!)}$$

Similarly, we can solve equation (7d) for T<sup>2</sup> and substitute this into equation 7c, giving us

where

$$E_{\#} = \frac{J(\lambda - \lambda_{\#})z_{!} + \lambda_{\#}(\lambda T + Jz_{\$})}{z_{!}(z_{\$} - z_{!})a_{+}q_{!}a_{\%}q_{\$}}$$

Equations 14a and 14b represent the governing convective heat transport equations that are solved below using finite difference methods.

#### S4. Numerical Methods

For the interior part of the solution domain near the origin, we were unable to solve equations 14a and 14b analytically. We approximated the solution using the finite difference method. We used an unwinding scheme for the cross derivatives to avoid numerical oscillations. Letting  $\Delta y = \Delta x$ , the finite difference numerical approximation for T<sup>2</sup> is given by:

)<sup>#</sup>;)<sup>#</sup>;)<sup>#</sup>,)<sup>#</sup>;)<sup>#</sup>

$$\frac{4.6 - 47!.6 - 4.67!}{\Delta^{*}} + D_{\#} \frac{4.6 - 47!.67}{\Delta^{*}} + D_{+} \frac{4.6 - 4.67!}{\Delta^{*}} + D_{,} T_{D,?}^{!} = D_{\%}T_{.} + D_{\&}J_{.}$$
(15)

where

$$D_{\#} = \frac{\lambda . T_{-}}{(z_{\$} - z_{!})a_{\%}q_{\$}} \qquad D_{+} = \frac{(\lambda \# - \lambda)\lambda \# + \lambda \# Z_{\$}}{(z_{\$} - z_{!})a_{\%}q_{\$}} \qquad D_{,} = \frac{\lambda . \lambda \#}{z_{!}(z_{\$} - z_{!})a_{+}q_{!}a_{\%}q_{\%}}$$

$$D_{\%} = \frac{\lambda \lambda \#}{z_{!}(z_{\$} - z_{!})a_{+}q_{!}a_{\%}q_{\$}} \qquad D_{\&} = \frac{\lambda}{a_{\%}q_{\$}(z_{\$} - z_{!})}$$

Grouping like terms:

$$(1 + \Delta x D_{\#} + \Delta x D_{+} + \Delta x^{+} D_{.}) T_{D,?}^{!} - (1 + \Delta x D_{\#}) T_{D,?,?}^{!} - (1 + \Delta x D_{+}) T_{D,?,;\#}^{!} + T_{D,\#,?,\#}^{!} = \Delta x^{+} [D_{\%} T_{-} + D_{\&} J_{.}]$$
(16)

We used a Point Jacobi iteration scheme to find our solution:

$$T! = \frac{\Delta^{*"}[F_{\&})_{0} > F_{*}7(] > (\# > \Delta^{*}F_{!}))_{47!,6}^{\#} > (\# > \Delta^{*}F_{"}))_{4,67!}^{\#}}{(\# > \Delta^{*}F_{!} > \Delta^{*}F_{"}) > \Delta^{*"}F_{!}}$$

$$D? \qquad (\# > \Delta^{*}F_{!} > \Delta^{*}F_{"} > \Delta^{*"}F_{!})$$

$$(17)$$

Person et al.

We solved for the temperatures in the confined aquifer  $(T^4)$  a similar fashion:

$$)^{\$};)^{\$};)^{\$} >)^{\$};)^{\$}$$

$$\frac{4.6 + 47!.6 + 4.67! + 47!.67!}{\Delta^{*}} + D_{\#} + \frac{4.6 + 47!.6}{\Delta^{*}} + D_{\#} + \frac{4.6 + 4.67!}{\Delta^{*}} + D_{\#}, T_{D,?}^{\$} = E_{\#}$$
(18)

Person et al.

Grouping like terms:

$$(1 + \Delta x D_{\#} + \Delta x D_{+} + \Delta x^{+} D_{,}) T^{\$}_{D,?} - (1 + \Delta x D_{\#}) T^{\$}_{D,\sharp \#,?} - (1 + \Delta x D_{+}) T^{\$}_{D,?;\sharp} + T^{\$}_{D,\sharp \#,?;\sharp} = \Delta x^{+} E_{\#}$$
(19)

Using a Point Jacobi iteration scheme, we have:

$$T^{\$} = \frac{\Delta^{*"}H_{!} > (\# > \Delta^{*}@")_{\flat}^{\$}_{7!,6} > (\# > \Delta^{*}A")_{\flat}^{\$}_{67!};)^{\$}_{47!,67!}}{(\# > \Delta^{*}F_{!} > \Delta^{*}F" > \Delta^{*"}F')}$$
(20)

We iterated using equations (17) and (20) until convergence was reached.

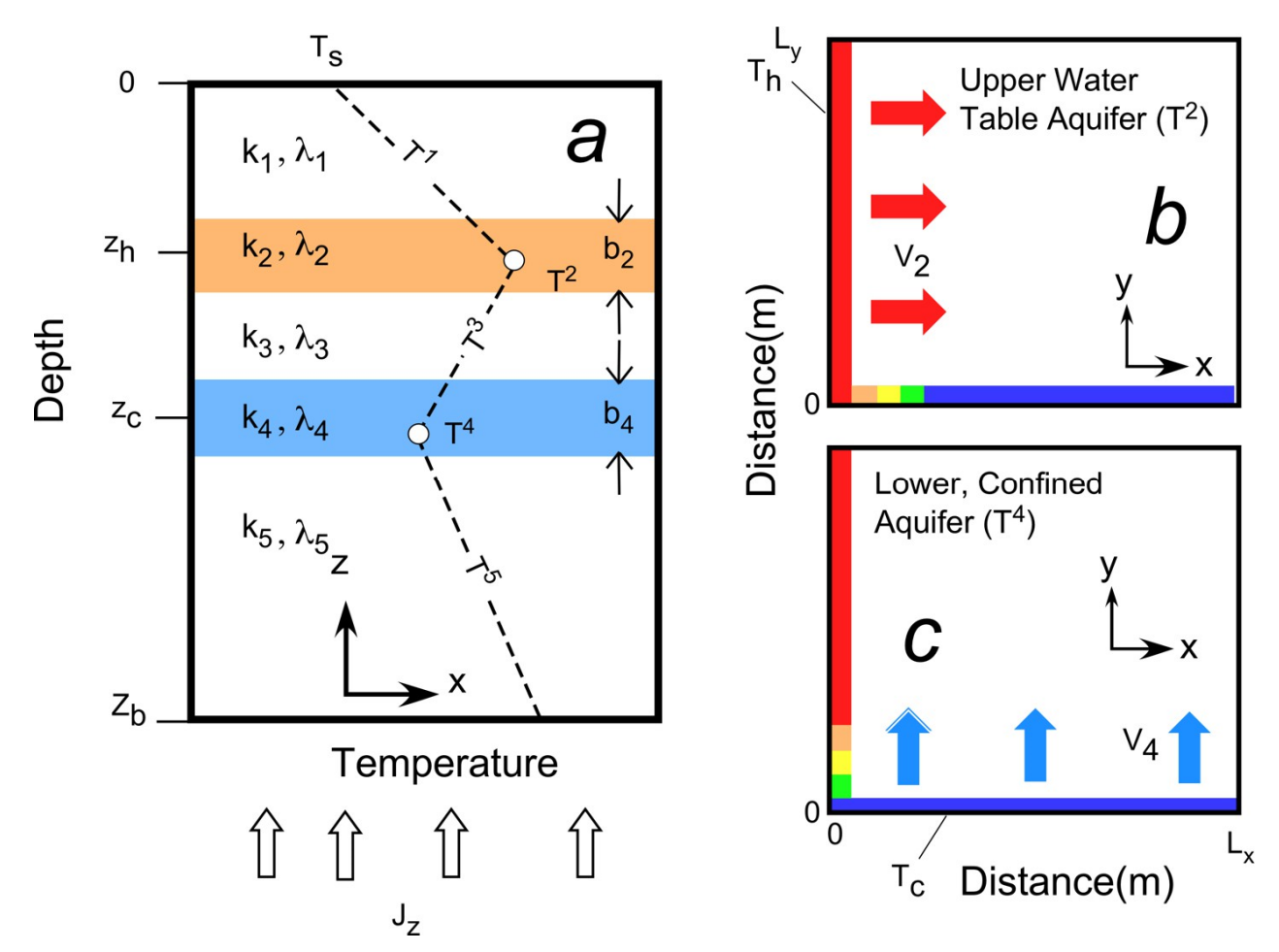


Figure S1. (a) Cross-sectional schematic diagram depicting variables used in the semi-analytical solution. Plane view images of the variables used in the upper and lower aquifers are shown in subplots (b) and (c), respectively. Note that temperature in the upper aquifer along the left edge (x=0,y) is fixed at  $T_h$ . An analytical solution is used to impose temperatures along the lower boundary (x, y=0) of the upper aquifer. (d) Flow system in the lower confined aquifer. The temperature along the bottom edge of the confined aquifer is fixed at  $T_c$ . An analytical solution is used to specify the temperature along the left edge (x=0, y) of the confined aquifer. The flow directions are depicted by the arrows. The thermal conductivity of the five layers are denoted by  $\lambda_1 - \lambda_5$ , respectively. The permeability of each layer is denoted by  $k_1$ - $k_5$ , respectively. The basal heat flux is denoted by the variable  $J_z$ .

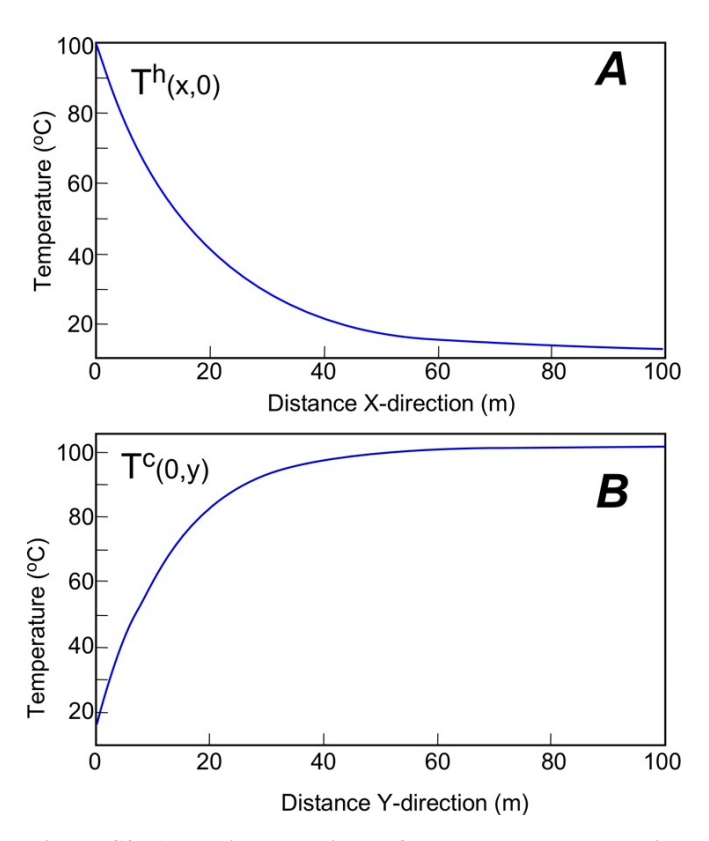


Figure S2. Analytical solutions of temperature versus distance for the upper (A) and lower (B) aquifers from Run 4.

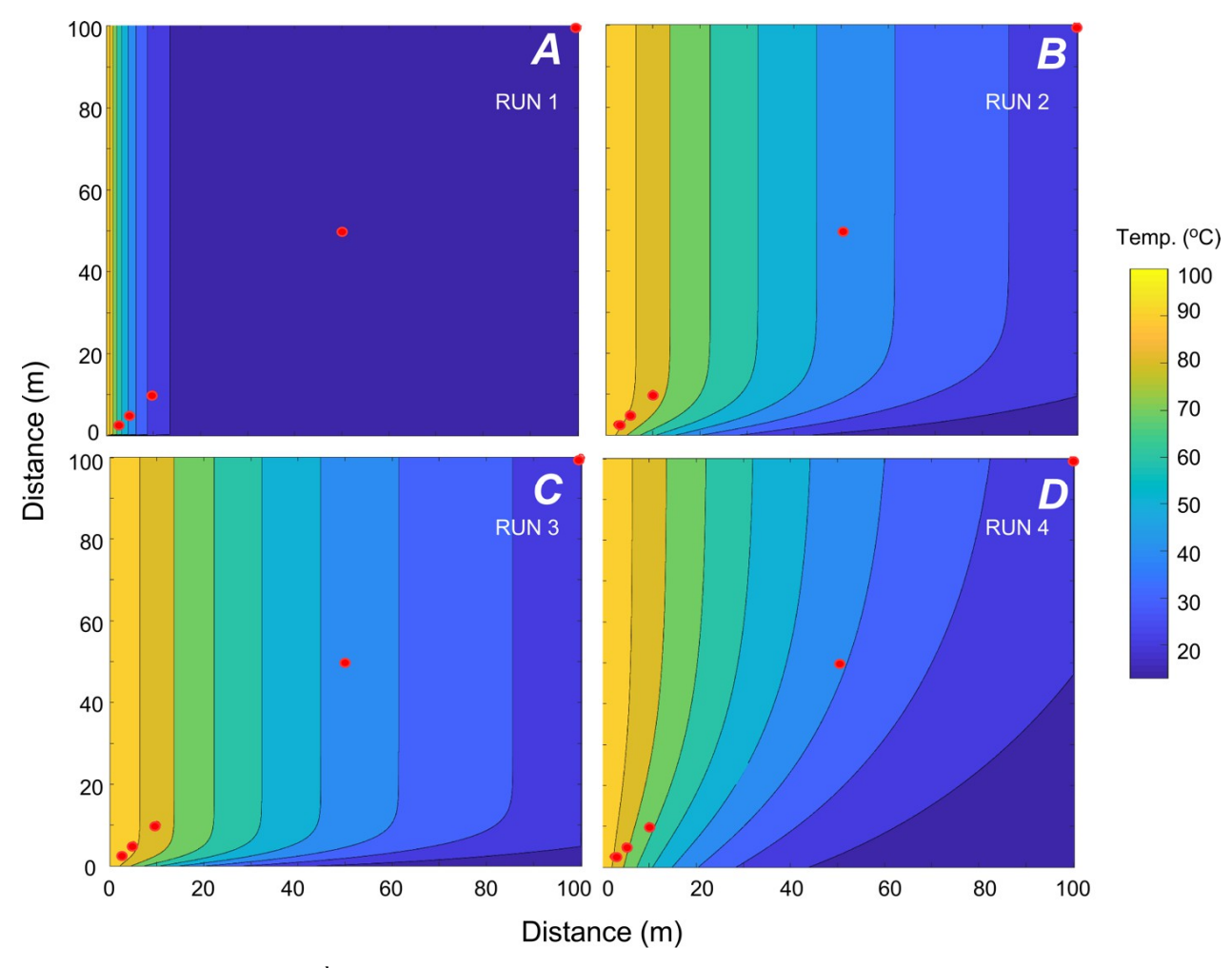


Figure S3. Temperature  $(T^h)$  contour plots for the upper aquifer. The red dots depict the locations of the temperature profiles shown in Figure 3.

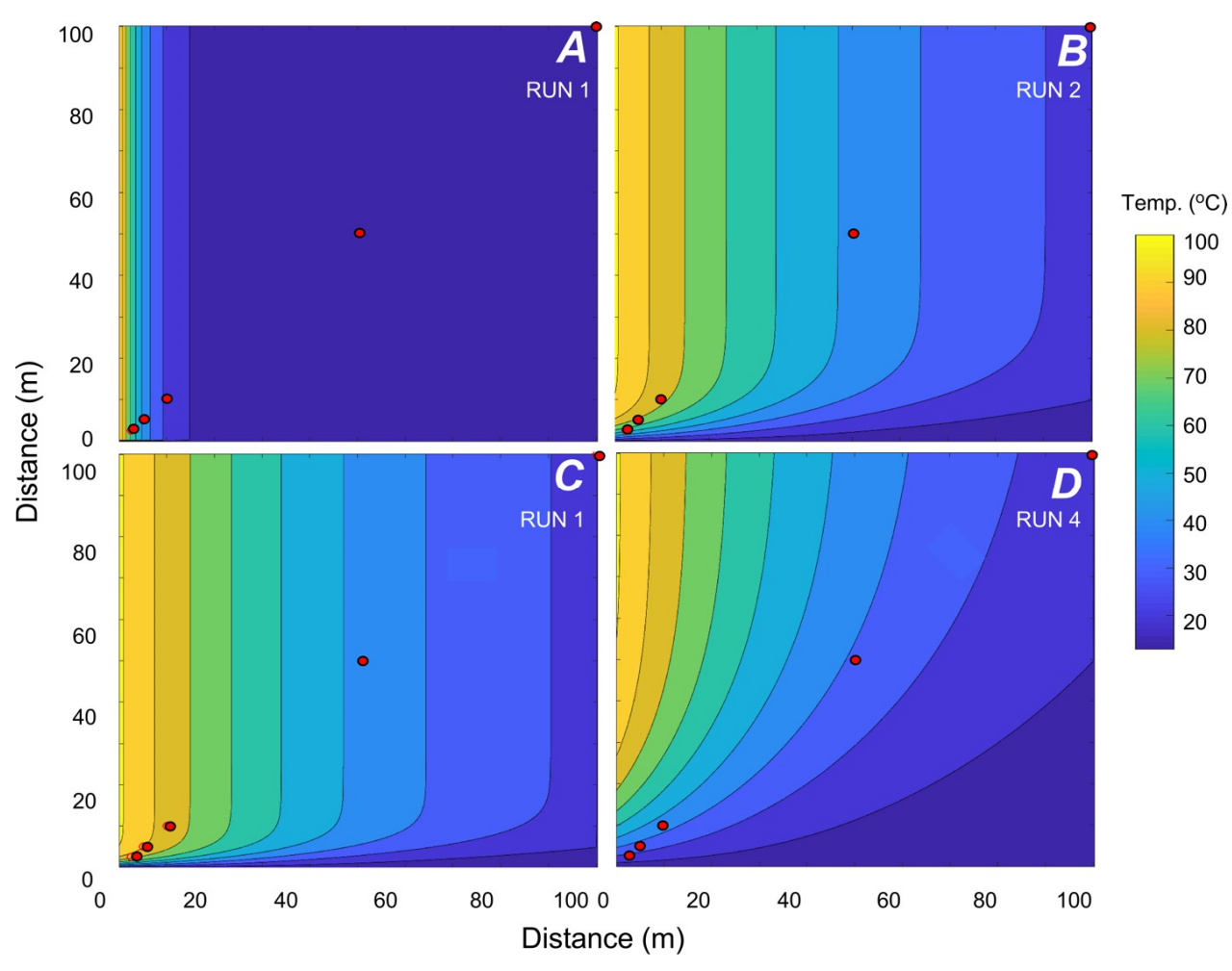


Figure S4. Temperature (T<sup>c</sup>) contour plots for the lower aquifer. The red dots depict the locations of the temperature profiles shown in Figure 3.